ISTITUTO NAZIONALE DI FISICA NUCLEARE

Sezione di Torino

INFN/AE-95/14
31 Maggio 1995

G. Bassompierre, G. Bologna, D. Boget, M. Chevallier, S. Costa, J. Dufournaud, M. Farizon, B. Farizon Mazuy, A. Feliciello, M.J. Gaillard, R. Garfagnini, R. Genre, M. Gouanère, B. Ille, R. Kirsch, P. Lautesse, M. Richard, E. Rossetto, D. Sillou, M. Spighel:

SEARCH FOR LIGHT NEUTRAL OBJECTS PHOTOPRODUCED IN A CRYSTAL STRONG FIELD AND DECAYING INTO $e^+ - e^-$ PAIRS

Accepted for publication in **Physics Letters B**

PACS: **12.20.D; 14.80.G; 14.80.Pb; 61.80.M**
Keywords: **QED strong field. Very light bosons. Channeling.**

SIS-Pubblicazioni
dei Laboratori Nazionali di Frascati

INFN – ISTITUTO NAZIONALE DI FISICA NUCLEARE
Sezione di Torino

INFN/AE–95/14
31 Maggio 1995

Search for light neutral objects photoproduced in a crystal strong field and decaying into e^+e^- pairs

G. Bassompierre[a], G. Bologna[b,1], D. Boget[a], M. Chevallier[c], S. Costa[b,2], J. Dufournaud[a], M. Farizon[c], B. Farizon Mazuy[c], A. Feliciello[b,3], M.J. Gaillard[c], R. Garfagnini[b,4], R. Genre[c], M. Gouanère[a], B. Ille[c], R. Kirsch[c], P. Lautesse[c], M. Richard[a], E. Rossetto[b,3], D. Sillou[a], M. Spighel[a]

[a] *Laboratoire d'Annecy-Le-Vieux de Physique des Particules IN2P3–CNRS, F–74941 Annecy-Le-Vieux Cedex, France.*

[b] *Università di Torino e INFN — Sezione di Torino — Via P. Giuria 1, I–10125 Torino, Italia.*

[c] *Institut de Physique Nucléaire de Lyon, IN2P3–CNRS et Université Claude Bernard, F–69622 Villeurbanne Cedex, France.*

Abstract

We describe a search for a light neutral object, X_0, possibly produced by $\approx$ 100 GeV photons interacting with the QED strong field encountered along the (110) axis of a cooled Ge crystal. We look at the e^+e^- decay mode, in short- (10^{-18} – 10^{-12} s) as well as long- (10^{-13} – 10^{-8} s) lifetime detection conditions. For a mass of 1.8 ± 0.2 MeV/c^2 ('Darmstadton' mass) we find no evidence for X_0 production. The upper limit for the ratio between e^+e^- decay rate and pair creation is given as a function of the X_0 lifetime. It reaches $\approx 5 \times 10^{-4}$ and $\approx 2 \times 10^{-5}$ in the short- and long-lifetime modes, respectively, including the crystal absorption contribution. However, for the long-lifetime mode and 10^8 incident photons, nine events are compatible with neutral objects having masses ranging from 2.1 to 3.5 MeV/c^2. A Monte Carlo simulation of the background gives only one event in the same energy range.

[1] Istituto di Fisica Generale, Università di Torino e Laboratori Nazionali dell'INFN, Frascati, Italy.

[2] Dipartimento di Fisica Sperimentale, Università di Torino e Sezione di Torino dell'INFN, Italy.

[3] Sezione di Torino dell'INFN, Italy.

[4] Istituto di Fisica Generale, Università di Torino e Sezione di Torino dell'INFN, Italy.

1 Introduction

Two experiments (EPOS and ORANGE) [1–4] performed at GSI, Darmstadt, have detected narrow lines (50 keV FWHM) in the energy spectrum of positrons emitted in collisions of heavy ions ($\approx$ 5.8 MeV/u) with heavy atoms, superimposed on the expected broad e^+ energy distribution. Moreover, narrower peaks were observed in the energy sum spectrum of e^+e^- pairs emitted in the same collisions, indicating a compensation of individual Doppler effects. The e^+e^- energy difference was found to be centred at 0 ± 40 keV with FWHM $\leq$ 260 keV. The additional observation of angular correlations between e^+ and e^- led the two groups to assume the creation of a neutral particle X_0 ('Darmstadton') decaying into a back-to-back ($180° \pm 18°$) e^+e^- pair, and having a mass of $\approx$ 1.8 MeV/c^2. Limits to its lifetime were set at 10^{-17} s $< \tau < 10^{-9}$ s.

Many experiments of different types have been performed when searching for such a particle. No signal was observed in Bhabha scattering [5] or in two-photons annihilation-in-flight experiments [6]. Upper limits were established for the partial widths $\Gamma_{e^+e^-}$ and $\Gamma_{\gamma\gamma}$, corresponding to a lifetime longer than 3.5×10^{-12} s. Furthermore, the negative results of beam-dump experiments [7] exclude longer lifetimes. Explanations of the GSI observations in terms of atomic or nuclear processes can also be excluded [8].

The following assumptions have been suggested for reconciling the GSI results with these negative results:

a) The X_0 is not elementary. It could have an extended size (100–1000 fm) implying an internal structure [9].
b) An external strong electromagnetic field is required for
   b1) the production of the X_0 and/or
   b2) its decay into an e^+e^- pair. In this case $\Gamma_{e^+e^-}$ should depend on the external field [10].
c) The photoproduction and/or decay proceed through a multistep mechanism [11]. These processes decouple input and output channels so that the time reversal cannot be applied.

One can point out that assumptions a), b) imply that beam-dump experiments are inconclusive. In particular, an extended object might not emerge from 'amorphous' materials. Similarly, assumptions b), c) make Bhabha scattering experiments inconclusive. Indeed, in these one-step process experiments, strong field conditions are not present, preventing the X_0 from being produced.

As a matter of fact, the existence of an extented object, with a lifetime 10^{-17} s $< \tau < 10^{-9}$ s, produced in a strong field in a relatively 'transparent' target, is not excluded by any existing experimental result.

The requirements of strong field and transparency can be satisfied by using a technique already exploited by some of us. Indeed, previous experiments [12] at CERN measured the cross-section for the process

$$\gamma + \text{crystal} \rightarrow e^+e^- + \text{crystal} \ , \tag{1}$$

i.e. the direct e^+e^- pair production from high-energy photons ($\approx$ 100 GeV) interacting with the strong macroscopic field existing along the $\langle 110 \rangle$ axis of a cooled Ge crystal. These experiments provided clear evidence that a single crystal is a very efficient source of a strong electromagnetic field. In addition, because of the periodic lattice structure, to extended objects a crystal should be more transparent than an amorphous material.

Guided by these considerations, in the present experiment we search for the e^+e^- decay of a light ($\approx 2\ \text{MeV}/c^2$) neutral particle, X_0, possibly produced in the process

$$\gamma + \text{crystal} \rightarrow X_0 + \text{crystal} \ . \quad \Big\lfloor_{\rightarrow e^+e^-} \tag{2}$$

However, if a final interaction were necessary to induce the decay of the X_0 [assumption b2) above], a negative result from our experiment would still be inconclusive.

A more detailed discussion justifying the possible occurrence of process (2) is given in Section 2. The dominant background source to this process is simply process (1).

Some results from this experiment have already been published [13].

2 Strong fields in heavy ion–heavy atom collisions and in high-energy photon–crystal interactions

The γ-crystal interaction in macroscopic strong field conditions is mediated by a multiphoton process. The same process occurs in the photon-microscopic strong field interaction in heavy ion–heavy atom (HIA) collisions [11]. In the latter case the strength of the field can be characterized by the parameter $Z\alpha$, where $\alpha = 1/137$ is the fine structure constant. The Coulomb field created by the two colliding nuclei (corresponding to $Z = Z_1 + Z_2 \approx 184$, as in the case of the GSI experiments) is strong, as $Z\alpha > 1$; therefore the $1s_0$ state is bound with a value $E_{\text{bound}} < -m_0c^2$, allowing induced and spontaneous positron creation. During the interaction the time-dependent Coulomb field lasts for

only $\approx 2 \times 10^{-21}$ s and is equivalent to a photon of ≈ 300 keV, which can induce pair creation (IPC). Figure 1a illustrates IPC in HIA collisions, while Fig. 1b represents IPC in the crystal case. In both diagrams the interaction proceeds through the exchange of many photons. In the HIA case, one of these virtual photons transfers its energy, $h\nu$, to the system:

$$h\nu = T_{e+} + T_{e-} + V_{e+} + V_{e-} + 2m_0c^2 \ ,$$

where T_{e+}, T_{e-}, V_{e+}, V_{e-} are the kinetic and potential energies of the e^+ and e^- that can be created at different points (non-local production [14]). The spontaneous pair production corresponds to the case where $V_{e+} + V_{e-} + 2m_0c^2 < 0$.

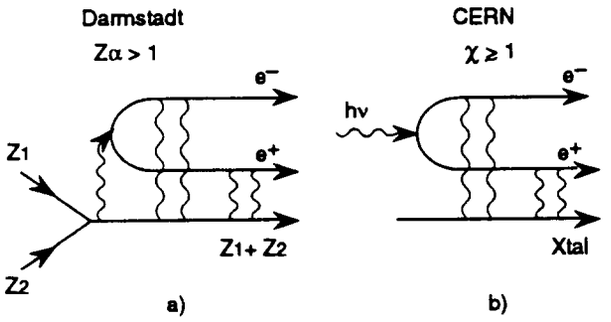

Fig. 1. Induced pair creation in strong fields.

In the crystal case, the field can be thought of as having a continuous cylindrical symmetry around a crystal axis, to which the field is perpendicular [15]. We may write an equation similar to the previous one for the potential of this macroscopic, uniform transverse field in the transverse plane:

$$k_\perp^2/2k = V_{e+} + V_{e-} + \left(m_0^2c^4 + p_{\perp e+}^2c^2\right)/2p_{e+}c + \left(m_0^2c^4 + p_{\perp e-}^2c^2\right)/2p_{e-}c \ ,$$

where $k_\perp$ and k are the transverse and total energies of the incident photon. In the case of perfect alignment ($k_\perp = 0$) we can observe only the spontaneous pair creation. In our experiment, high-energy (≈ 100 GeV) real photons are sent parallel to the crystal axis, where they feel a strong field. A formation length [16] L_f is necessary for the production of a mass M. L_f is the pathlength corresponding to a lag of the neutral particle behind the photon equal to $\lambda\!\!\!^{-} = \hbar c/k$, the reduced wave length of the photon. For $k = 100$ GeV photons and $M = 1.8\ \mathrm{MeV}/c^2$, $L_f = 2\hbar ck/(Mc^2)^2 \approx 12$ nm (≈ 30 atoms). This justifies the assumption that the field is continuous. Let $\mathcal{E}$ be its mean value, which can reach 1.5×10^4 V/nm. The parameter characterizing the field strength is now:

$$\chi = \gamma\mathcal{E}/\mathcal{E}_c \ , \quad \text{where} \qquad \gamma = k/2m_0c^2 \ , \quad \mathcal{E}_c = m_0^2c^3/e\hbar \ ;$$

$\mathcal{E}_c = 1.33 \times 10^9$V/nm is called the critical field: if $\gamma\mathcal{E} \approx \mathcal{E}_c$ (i.e. $\chi \approx 1$), the static, uniform transverse field $\mathcal{E}$ is sufficiently strong to allow the creation of an e^+e^- pair in vacuum. This is qualitatively shown by the following quasi-classical argument: for particles created with equal momenta p, almost collinearly with the photon (within a small angle $1/\gamma$), longitudinal momentum conservation in vacuum requires $k \approx 2\ pc$. Newton's law of motion requires $\Delta p_\perp = e\mathcal{E}\Delta t \approx m_0 c$ ($k \gg m_0c^2$), where $e\mathcal{E}$ is the absolute value of the transverse force and m_0c is the absolute value of the particle transverse momentum acquired during the pair formation time Δt. There is then an energy violation $\Delta E = 2(p^2c^2 + m_0^2c^4)^{1/2} - k \approx m_0c^2/\gamma$ that can be tolerated during the time interval Δt, provided it is smaller than the energy fluctuations governed by the uncertainty principle. This corresponds to the requirement $\Delta E\ \Delta t < \hbar$, or $\chi > 1$.

The similarity between the two cases can be seen by comparing the IPC probabilities, $P_{\rm IPC}$, when the strong field conditions are fulfilled. In HIA collisions, $P_{\rm IPC}$ is the ratio between the measured cross-section $\sigma_{\rm IPC}$ for IPC and the geometrical cross-section $\sigma_{\rm geom}$ involved in strong field conditions; $\sigma_{\rm IPC} \approx$ 2 mbarn, $\sigma_{\rm geom} \approx 12$ barn for an impact parameter ≈ 20 fm. Then $P_{\rm IPC} = 1.7 \times 10^{-4}$ at $Z_1 + Z_2 = 184$. For γ-crystal interactions, the pair creation cross-section per unit length [17] in the uniform field approximation defines a pair creation length $L_{\rm IPC}$. We can see that $P_{\rm IPC} = L_f/L_{\rm IPC}$. For $\mathcal{E} \approx 10^4$ V/nm and $k = 100$ GeV, $\chi = 0.75$, $L_{\rm IPC} = 0.02$ cm and $P_{\rm IPC} = 1.9 \times 10^{-4}$. The two probabilities $P_{\rm IPC}$ are of the same order of magnitude. Note that in HIA collisions the ratio between the production of positrons falling in the narrow energy lines and in the expected, broad distribution is $\approx 3\%$.

3 Experimental set-up

The experimental apparatus is sketched in Fig. 2. We note that the distances are not to scale.

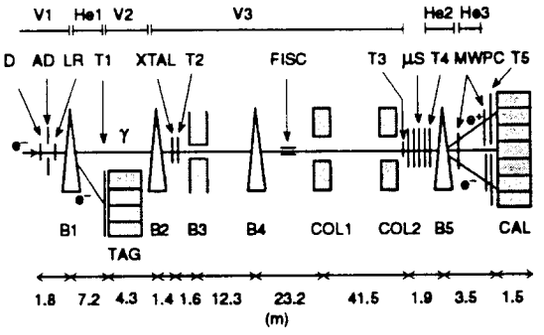

Fig. 2. Experimental set-up, seen from above. The distances are not to scale.

3.1 Beams

The CERN–SPS 450 GeV proton beam hits a beryllium target (not shown in Fig. 2). The emerging charged particles are swept away by a magnetic field. The neutral component — mainly photons from π_0 decay — hits a second target; the electrons of the photoproduced e^+e^- pairs are momentum-selected ($p = 150$ GeV/c, $\Delta p/p \approx 3 \times 10^{-3}$). A high purity electron beam is obtained by synchrotron radiation effect: the hadron/muon contamination is reduced from $\approx 1\%$ to $\sim 10^{-4}$. The beam has a low angular divergence with an rms value of 64 μrad. The beam cross-section at the entrance of the experimental area is 50 mm^2 and the intensity is $\approx 2 \times 10^5$ e^- per burst. The burst duration is ≈ 2 s [18].

Two circular scintillators, D1, D2 (diameter 12 mm, thickness 1 mm), and a hole-scintillator, AD (diameter 8 mm, thickness 4 mm), define the e^- beam, which hits a 0.5 mm thick lead radiator LR. The resulting photon beam γ is tagged by bending the outgoing electrons, using magnet B1, and these are detected with four total absorption counters (TAG). Each counter (106 × 106 × 450 mm^3) is made of SF6 lead glass and can be moved into the incident e^- beam for calibration purposes. A scintillator slab T1 (315 × 26 mm^2), parallel to the front face of the TAG counters, is used in coincidence. The corresponding energy range of the tagged γ-ray beam is 83–133 GeV.

The electron–photon beam line runs in vacuum pipes in regions V1 (from the SPS machine to the exit of B1), V2 (along the tagging system) and, finally, V3 (from the tagging system to the position sensitive detector μS, 83 m farther). Between B1 and the tagging system, photons and electrons pass through a large helium bag, He1. Just in front of the crystal (XTAL), a magnet, B2, eliminates pairs produced upstream in the helium bag or in surfaces limiting the helium bag and the vacuum pipes.

3.2 Experimental apparatus

The 0.42 mm-thick Ge single crystal (XTAL) is mounted on a two-axis goniometer which can rotate by steps of 1.4 μrad. The goniometer can be moved along two perpendicular axes. The target holder was linked to a liquid nitrogen reservoir and the temperature of the crystal was close to 100 K, while the temperature of the goniometer was maintained at 290 K. A scintillator, T2, could be inserted in the beam line to detect the e^+e^- pairs produced in the crystal.

The magnets B3 and B4 are used in one of the experimental conditions (the long lifetime mode — see Section 4). The magnet B3 has a high bending power

($\approx$ 1.7 Tm). It vertically deflects e^+ and e^- originating from the crystal. The magnet B4, located 12.3 m downstream, has a low bending power (BL $\approx 8 \times 10^{-3}$ Tm). It imparts to charged particles a small kick in the horizontal plane (see Subsection 4.2).

The vacuum pipe in region V3, maintained at a pressure of $\sim 10^{-2}$ Pa, ends with a mylar window 0.1 mm thick, and is shielded against the earth's magnetic field by a μ-metal tube. The residual magnetic field, normally less than 10^{-6} T, is slightly higher ($\sim 10^{-5}$ T) near two FISC (finger counter) systems used to control the beam position. An iron collimator, COL1 (400 mm thick, hole 56 mm in diameter), is located 41.5 m before a position-sensitive detector μS; another identical collimator, COL2, is located just in front of μS.

The microstrip silicon detector [19] μS (50 μm pitch), located 83 m from XTAL, consists of four parallel plates (20 $\times$ 20 mm^2, each 0.3 mm thick) and performs a double measurement of the x and y positions of charged particles. A small counter, T3 (14 $\times$ 14 $\times$ 1 mm^3), is used for beam alignment, while counter T4 (21 $\times$ 21 $\times$ 2 mm^3) is used to start the readout of the μS detector.

Behind the μS detector a magnetic analysis of the e^+ and e^- momenta is performed in the horizontal plane by magnet B5. The e^+ and e^- tracks are reconstructed using three Proportional Chambers (MWPC), each with a surface of 80 $\times$ 206 mm^2, and consisting of two vertical wire planes. The wire pitch is 1 mm and there is a 0.5 mm offset between the two planes. Two helium bags, He2 and He3, are used to reduce multiple scattering.

The last detector, CAL, is a calorimeter made of seven SF6 lead glass counters identical to the TAG counters. Two rectangular scintillators, T5, define the useful momentum acceptance of the calorimeter (11–116 GeV/c).

4 Experimental method

The experimental set-up was designed to be sensitive to X_0 masses between 1 and 4 MeV/c^2 by measuring the angle θ between e^+ and e^- particles and their energies E^+ and E^-, in the 11–116 GeV range. The X_0 mass M can be expressed as follows:

$$M^2c^4 = \frac{(\Delta p_\perp)^2c^2 + 4m_0^2c^4}{1-A^2} = \frac{k^2\theta^2}{4}(1-A^2) + \frac{4m_0^2c^4}{1-A^2} \ , \qquad (3)$$

where

$$\Delta p_\perp = |\mathbf{p}_{+\perp} - \mathbf{p}_{-\perp}| = |\mathbf{p}^*_{+\perp} - \mathbf{p}^*_{-\perp}|$$
$$= (M^2c^2 - 4m_0^2c^2)^{1/2} \ |\sin\theta^*| \approx \theta\frac{2E^+E^-}{kc} \qquad (4)$$

is the absolute value of the vector difference between the e^+ and e^- transverse momenta in the laboratory and X_0 rest frame, $k \approx E^+ + E^-(k \gg Mc^2)$ is the photon energy and $A = (E^+ - E^-)/(E^+ + E^-)$ is the energy asymmetry, which is related to θ^*, the emission angle of the e^- with respect to the incident photon in the X_0 rest frame, by the equation

$$A = \cos\ \theta^* \left(1 - \frac{4\ m_0^2}{M^2}\right)^{1/2} .$$

Here, momentum and energy are almost identical, due to the validity of the ultrarelativistic approximation.

For $Mc^2 = 1.8$ MeV and $k = 100$ GeV we obtain the minimum angle $\theta_{\text{min}} \approx 30\ \mu$rad. We measure the small separation $\Delta\rho$ between the impact points of the e^+ and e^- particles on the μS detector. For example, a decay occurring close to the target corresponds to $\theta_{\text{min}} \approx 30\ \mu$rad and will give $\Delta\rho \approx 2.4$ mm.

We are able to measure such small θ angles only if e^+ and e^- trajectories are not perturbed by stray and earth magnetic fields and by interactions with materials (see Subsection 3.2). The tolerable perturbation is $\leq 1\ \mu$rad. As a consequence, we cannot reconstruct trajectories by means of two position sensitive detectors and must measure θ using only one position-sensitive detector. However, in order to observe a weak signal from process (2), superimposed on the background from the direct process (1) and broadened by the effect of e^+ and e^- scattering in the crystal, the decay point has to be known with a precision (FWHM) of the order of 10% or better. For this reason, measurements were performed in two alternative experimental modes, as described below.

4.1 Short-lifetime mode

In the short-lifetime mode, the magnets B3 and B4 are carefully demagnetized at a few 10^{-6} T.

The distance between creation and decay point of the X_0 spans several orders of magnitude. Its lower limit is estimated to be $\sim 100\ \mu$m (due to the finite crystal thickness), while the upper limit is estimated to be ~ 10 m. Correspondingly, the order of magnitude of the spanned lifetime interval is $5 \times 10^{-17}\ \text{s} < \tau < 10^{-12}\ \text{s}$. The uncertainty in θ is estimated to be $\Delta\theta/\theta \approx \pm 7\%$ (or a standard deviation of $\approx 4\%$).

In this mode the magnet B3 (see Fig. 2) is used to sweep out all charged particles, in particular all the e^+e^- pairs originating in the crystal. The kicking magnet B4 is used to tag X_0 decay events occurring between B3 and B4. After identification of the sign of each charged particle and measurement of their energies, we measure the horizontal (vertical) separation Δx (Δy) between the impact points of the e^+ and e^- on μS. We then define the corresponding angles in the horizontal and vertical planes

$$\tilde{\theta}_x = \frac{\Delta x}{d} , \qquad \theta_y = \frac{\Delta y}{d} ,$$

where $d = 71$ m is the distance between the B3–B4 middle point and μS (the tilde on θ_x is used to remind us that the angle is magnetically perturbed). The horizontal and vertical projections of the transverse momentum difference are then given by — see Eq. (4):

$$\Delta\tilde{p}_{\perp x} = \tilde{\theta}_x \frac{2E^+E^-}{kc} , \qquad \Delta p_{\perp y} = \theta_y \frac{2E^+E^-}{kc} .$$

To obtain $\Delta p_{\perp x}$, the unperturbed transverse momentum difference in the horizontal plane, we must apply the appropriate magnetic correction 600 BL. The BL $\approx 8 \times 10^{-3}$ Tm value (see Subsection 3.2) has been chosen in such a way to select a few MeV/c^2 of the X_0 mass range ($\approx 1-4$ MeV/c^2). We have

$$\Delta p_{\perp x} = \Delta\tilde{p}_{\perp x} - 4.8 \text{ MeV}/c .$$

This correction is inappropriate for events corresponding to decays after B4. It leads to incorrect masses and destroys the natural azimuthal symmetry. On the contrary, the group of events corresponding to decays occurring before B4 will show an azimuthal symmetry only after the magnetic correction. Consequently, by azimuthal symmetry considerations, we have the possibility of classifying the events in two groups corresponding to these two decay zones (see Subsection 5.2.2). Since the pairs produced in the crystal have been removed by the magnet B3, the events produced between B3 and B4 are expected to give rise to a clean mass spectrum with no background coming from the crystal and no distorsion due to a wrong magnetic correction.

The X_0 mass M is obtained by introducing the experimental values of $(\Delta p_\perp)^2 = (\Delta p_{x\perp})^2 + (\Delta p_{y\perp})^2$ and A in Eq. (3). The uncertainty in mass determination is estimated to be $\Delta M/M = \pm 8.7\%$ (a standard deviation of 5.0%).

5 Data analysis and experimental results

An event is considered if the distance between two hit strips of the μS detector in both the horizontal and vertical directions is larger than 0.2 mm. The e^+ and e^- tracks are reconstructed before the B5 magnet in both the horizontal and vertical plane using the μS detector, and after B5 in the horizontal plane using only the MWPCs. In order to associate the two track segments which correspond to the same trajectory in the horizontal plane, we extrapolate all horizontal tracks to the centre of B5 and choose the association giving the smaller value for the variable a, defined as the sum of the two distances between the extrapolated coordinates. Figure 3a shows the distribution of the smaller value of a. The distribution of the larger value, corresponding to the wrong association of track segments, is shown in Fig. 3b.

An event is accepted if the smaller value of a is $\leq$ 1.4 mm. From the two distributions of Figs. 3a and 3b we estimate that the fraction of rejected events is 5% and the fraction of accepted events containing a wrong association of track segments is 0.8%.

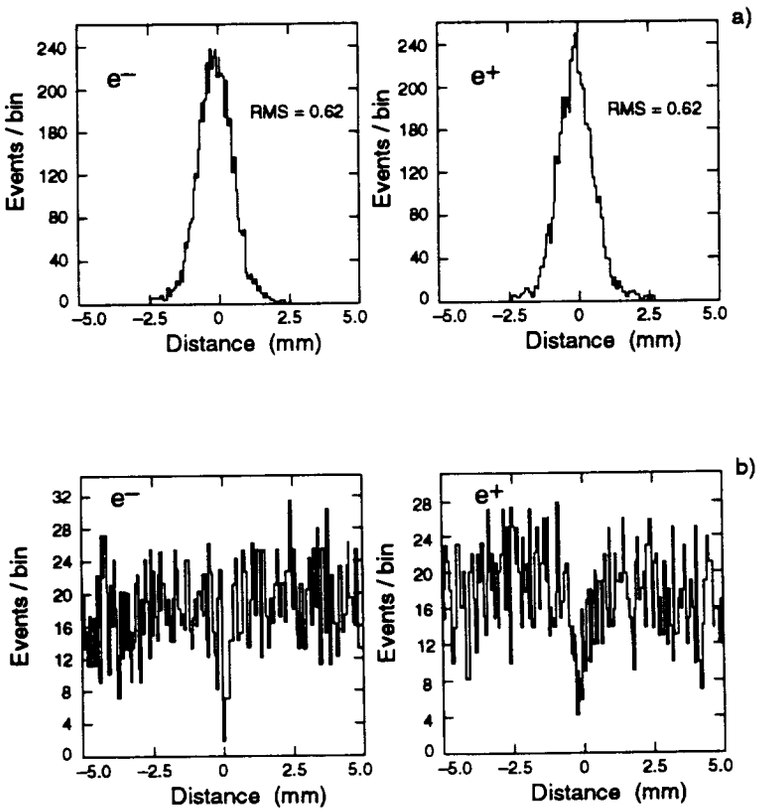

Fig. 3. Distribution of distances between extrapolated positions from μS and MWPC, for e^- and e^+: a) good choice, b) bad choice.

We have measured [20] the angular and energy distributions of e^+e^- pairs photo-produced in the aligned Ge crystal. After production, the e^+ and e^- interact both incoherently and by strong field effect with the crystal. The distributions are observed to depend on the angle between the incident beam direction and the $\langle 110 \rangle$ axis, as shown by performing measurements under both tight alignment and slight misalignment conditions. In the latter case, for a misalignment of 60 μrad, the asymmetry between e^+ and e^- angular distributions is $\approx$ 60 μrad.

To understand these results, we have performed a Monte Carlo simulation in the strong field using an existing program [21]. This simulation has no adjustable parameter and includes the choice of the pair production point in the crystal, the radiation energy loss, the angular perturbation of the e^+ and e^- trajectories in the crystal by multiple scattering and channelling phenomena. They indicate that the 60 μrad angular shift observed between the e^+ and e^- distributions is due to a misalignment of 60 μrad [20]. During data taking we verified that even with a misalignment of 60 μrad, the e^+e^- pair counting rate had the appropriate value for the strong field condition [12]. A Monte Carlo simulation using the EGS4 code [22] was also carried out for an 'amorphous' Ge slab of the same thickness as the crystal.

The experimental mass spectrum obtained in close alignment condition (20% of events) and with $\approx$ 60 μrad misalignment of the crystal (80% of events) is compared with the Monte Carlo simulations in Fig. 4 (see also [13]). The 'crystal' Monte Carlo simulation (continuous line) is in substantial agreement with the experimental data, while the 'amorphous' one (dashed line) shows, of course, a big discrepancy, which clearly demonstrates the dramatic impact of the strong field properties. The experimental mass distribution corresponds to a mean apparent mass $\overline{M}_{\rm exp} = 4.63$ MeV/c^2, to be compared with the corresponding calculated value $\overline{M}_{\rm MC} = 4.84$ MeV/c^2 for the continuous line, with an rms deviation of 2.07 MeV/c^2 to be compared with the corresponding calculated value of 2.11 MeV/c^2. The Monte Carlo 'amorphous' and 'crystal' simulated mass spectra contains 4.5×10^4 and 2.8×10^3 events, respectively, and are normalized to the experimental one. This contains 2.2×10^5 pairs analysed without ambiguity, corresponding to 8×10^8 incident electrons in the primary beam, 4×10^7 tagged photons and 2×10^6 pairs produced in the crystal. The last number corresponds to an overall detection efficiency of 0.11, which results from the acquisition dead time (0.72), the geometrical acceptance of the microstrips detector μS(0.31), the μS and MWPC efficiencies (0.90 and 0.73, respectively), and the analysis efficiency (0.75) due to the rejection of the ambiguous events.

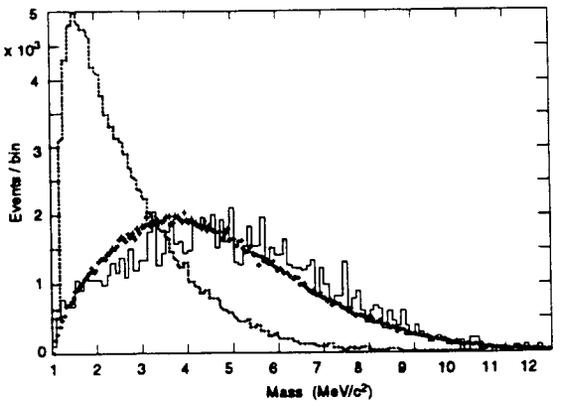

Fig. 4. Experimental mass spectrum and Monte Carlo simulations normalized to experimental data, for the short lifetime mode. Experimental data (dots): 2.2×10^5 events. 'Amorphous' Monte Carlo simulation (dashed line): 4.5×10^4 events. 'Crystal' Monte Carlo simulation (continuous line): 2.8×10^3 events.

We are looking for a narrow structure around 1.8 MeV/c^2. The experimental resolution results from the folding of two inaccuracies: detector resolution ($\approx$ 3%) and uncertainty in the decay point. Consequently, the effective mass resolution function depends on the X_0 lifetime.

The mass spectrum shows no statistically significant structure. In order to extract a possible signal at 1.8 MeV/c^2, we have used various cut-off values in the total energy spectra $E^- + E^+$ (60 to 120 GeV), in the relative $E^- + E^+ - k$ missing energy spectra (5 to 30%) and in the asymmetric distributions of angles between the trajectories of e^+ and e^-. The mass spectra modified by these cut-off values have also shown no structure.

Let R be the ratio of the number of X_0 to the number of e^+e^- pairs produced in the crystal strong field. The crystal transparency T for the X_0 is probably less than 100% and therefore in our experiment we can only measure the value of the product RT. Figure 5 shows the dependence on τ of u_{RT}, the 95% confidence level upper limit on RT. This limit reaches the value 4.5×10^{-4}, which is lower than the R value from the GSI experiments. The value of u_{RT} increases for $\tau < 10^{-16}$ s since the decay occurs before emergence from the crystal (in this case the uncertainty in mass determination, due to the properties of particle scattering in the crystal [20], is larger than 250 keV/c^2), with a probability increasing when τ decreases. The limits on the lifetime given by the Bhabha scattering experiments are irrelevant in hypotheses b) and c) of Section 1.

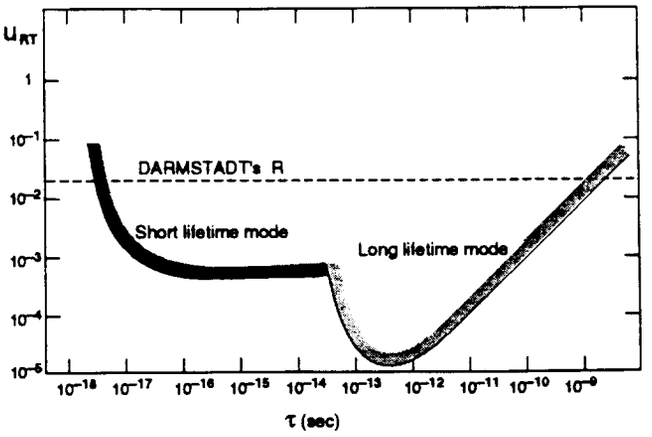

Fig. 5. u_{RT}, the 95% confidence level upper limit on RT for 1.8 MeV/c^2 X_0 production, versus lifetime τ for short and long lifetime modes. The dashed line indicates the R value measured at Darmstadt.

5.2 Long-lifetime mode

5.2.1 Background discussion and selection of candidates

In order to understand the background processes in the long-lifetime mode, the 'amorphous' Monte Carlo code (see Subsection 5.1) has the capacity to simulate the multiple photon production in the lead radiator RL and their successive interactions in the following materials (see Section 3 and Fig. 2).

Figure 6 shows the histograms of $\Delta\rho = (\Delta x^2 + \Delta y^2)^{1/2}$, Δx and Δy being the horizontal and vertical projection of the distance between the impact points on μS, obtained from the experimental data (circles) as well as from the Monte Carlo simulation (continuous lines). One sees that the simulated and experimental data are in good agreement for small $\Delta\rho(< 2$ mm). In this region, the Monte Carlo simulation shows that the main source of background consists of pair creation in the matter just before the μS (the last mylar window limiting the vacuum pipe V3, the scintillator T3 and the 15-cm air gap between the mylar window and μS). This explains the small distance between the impact points. For larger $\Delta\rho$ values, the source of background is different: it is the double pair creation in the same material by double bremsstrahlung photons produced in the RL radiator. These events correspond to $\approx$ 10% of the single bremsstrahlung events (dark area — note the pseudolog scale). For some of these events, one e^+ and one e^- can be lost — either swept by B5 outside the acceptance of MWPC, or lost by MWPC inefficiencies. The simulation accounts for 41 such events for $\Delta\rho > 6$ mm, but the number observed is 139. This suggests something new is going on at large distances.

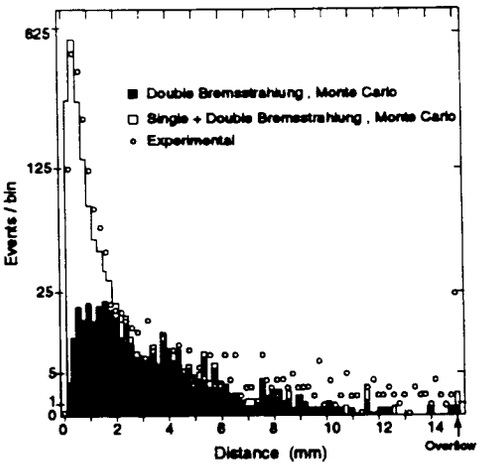

Fig. 6. Two-hits distance distribution; Δx, $\Delta y \geq 0.2$ mm. The pseudolog scale is given by α log $(1 + \beta N)$, where N is the number of events/bin and α, β are two adjustable parameters.

The confidence in our simulation has been strenghtened by studying e^+e^+ and e^-e^- pairs produced by double bremsstrahlung photons in events in which no e^+e^- pair was reconstructed because of inefficiencies. For the total event sample (see Subsection 5.2.2) nine same-sign pairs have been observed experimentally, in good agreement with the number of events predicted by the simulation program (11 events). We note that the measurements of same-sign pairs have been performed with the T5 signals removed from the trigger condition.

Special attention has been paid to looking at creation of pairs in the residual air of vacuum pipe V3, between magnets B3 and B4. The negligible multiple scattering they would suffer should give masses between 1 and 1.5 MeV/c^2 (see Subsection 5.2.2). But no event is observed between 1 and 2.1 MeV/c^2, even without any cut.

The other possible sources of background we can think of are:

a) Creation of pairs by the photon halo in the V3 pipe or in COL1. A separate Monte Carlo simulation which takes into account the measured photon halo gives no event for 10^9 incident electrons.
b) Creation of e^+e^- pairs from hadrons. As explained in Section 3, the hadronic contamination of the e^- beam is smaller than 0.1%. Hadroproduction, photoproduction or leptoproduction of neutral hadrons in the lead converter gives a maximum of 10^3 neutral hadrons for 10^9 incident electrons, leading to no pair being capable of simulating a good event. In addition, with our electromagnetic calorimeter, CAL, the rejection of events corresponding to a measured total energy lower than 130 GeV would decrease the corresponding background.

To summarize, the known sources of background cannot account for 139 − 41 = 98 events.

5.2.2 Mass Spectrum of the candidates

As already mentioned in Subsection 4.2, the events produced between B3 and B4 should exhibit an asymmetry in $\Delta\tilde{p}_{\perp x}$ before correction, but a symmetry around the point of coordinates $\Delta\tilde{p}_{\perp x} = 4.8$ MeV/c, $\Delta p_{\perp y} = 0$. Figure 7 shows the 139 events in the $\Delta\tilde{p}_{\perp x}$, $\Delta p_{\perp y}$ plane. To select the concerned candidates we have drawn a half-circle centred at $\Delta\tilde{p}_{\perp x} = 4.8$ MeV/c, with radius of 3.0 MeV/c. This radius has been chosen in such a way as to obtain the maximum uniformity in event distribution compatible with the maximum number of events. It is also consistent with our selection method for the mass range (see Subsection 4.2). Inside this half-circle one finds a group of nine events displaying the required azimuthal symmetry compatible with statistical fluctuations. These are the events that can then be thought of as originating from decays between B3 and B4. Outside this contour one counts a second group of 130 events presumably due mainly to X_0 decay between B4 and μS. The simulation gives a number of events from double bremsstrahlung equal to 1 inside the half circle, and to 40 outside. In addition (see Figs. 6 and 7), the distribution of single bremsstrahlung events is strongly peaked in the forward direction (smallest $\Delta\tilde{p}_{\perp x}, \Delta p_{\perp y}$).

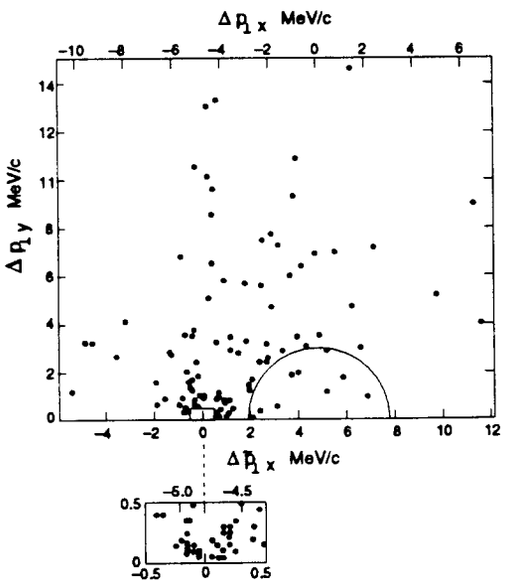

Fig. 7. Scatter plot of the 139 events in the transverse momentum plane; $\Delta x, \Delta y \geq 0.2$ mm. The small rectangle shows a magnified detail of the main plot. The nine events in the half-circle are attributable to decays occurring between the magnets B3 and B4.

Figure 8a shows the mass spectrum obtained for the 139 events and Fig. 8b the mass spectrum of the 41 events given by the Monte Carlo simulation. The magnetic correction is included in both spectra.

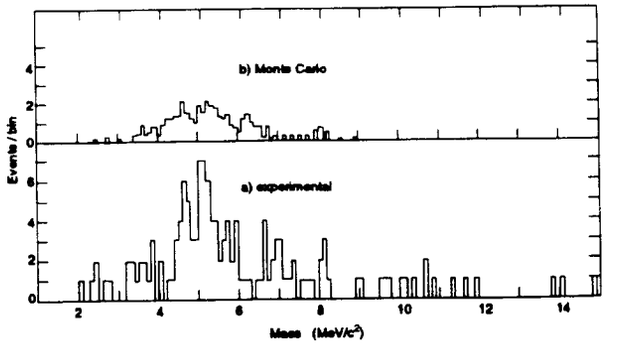

Fig. 8. a) Mass spectrum in long lifetime mode of the 139 events. b) Mass spectrum of the Monte Carlo background simulation. The vertical axis has been rescaled to take into account experimental efficiencies.

The following remarks can be made:

a) In the mass range close to 1.8 MeV/c^2, the value which corresponds to events seen at Darmstadt, there is no event at all, as in the short-lifetime mode.
b) We emphasize that the nine events compatible with the azimuthal symmetry have a mass ranging between 2.1 and 3.5 MeV/c^2. In the same mass range of the Monte Carlo spectrum one finds only one event. If we consider this value as an estimation of the true background, but allow for its fluctuation, the probability of nine or more events being a fluctuation of the background is 9×10^{-4}, on the basis of the compound Poisson distribution. This is a quantitative indication of the existence (or non-existence) of the X_0 in the mass range 2.1–3.5 MeV/c^2.
c) Candidates having a mass larger than 4 MeV/c^2 tend to have a wrong mass, as in this case the magnetic correction is perhaps inappropriate. These events should mainly correspond to decays after B4. So we make no claim on them.

Having no candidates in the 1.8 MeV/c^2 mass region and considering that the total number of 'potentially' detectable e^+e^- pairs should now be 5×10^5, corresponding to 2×10^9 incident electrons, 10^8 radiated photons and 5×10^6 effectively produced pairs, we again give in Fig. 5 the u_{RT} value, this time for the long-lifetime mode. For small values of τ, the decay occurs before the exit of B3, but if τ is too high, the probability of a decay between B3 and B4 is small. The minimum u_{RT} for this mode is $\approx$ 30 times lower than that for the short-lifetime mode.

6 Conclusion

The aim of this work was first to search for an hypothetical neutral object, X_0, of mass 1.8 MeV/c^2 decaying into e^+e^- pairs, the existence of which had been proposed to explain results obtained at GSI in heavy ion–heavy atom collision experiments. No event corresponding to this mass has been seen in either experimental mode. The 95% confidence limit for the product RT is given in Fig. 5. However, the mass spectrum obtained in the long lifetime mode contains nine candidates between 2.1 and 3.5 MeV/c^2, attributable to X_0 decays occurring between magnets B3 and B4. The sources of possible background have been extensively studied by Monte Carlo simulations. Only one event can be explained by double bremsstrahlung production.

Our indication for the existence of the X_0 between 2.1 and 3.5 MeV/c^2 relies on a Monte Carlo calculation. To be conclusive, an explicit measurement of the background with a misaligned crystal should have been done. This was indeed planned, but not accomplished, due to a tightened time schedule.

Acknowledgements

We are deeply indebted to F. Piuz for having provided us with the complete microstrip system.

References

[1] T. Cowan et al., Phys. Rev. Lett. **54** (1985) 1761; **56** (1986) 44.

[2] H. Tsertos et al., Z. Phys. **A326** (1987) 235; **A328** (1987) 129.

[3] W. K. Koenig et al, Phys. Lett. **B218** (1989) 12.

[4] P. Salabura et al., Phys. Lett. **B245** (1990) 153.

[5] S.M. Judge et al., Phys. Rev. Lett. **65** (1990) 972;
H. Tsertos et al., Phys. Lett. **B266** (1991) 259;
A.L. Hallin et al., Phys. Rev. **D45** (1992) 3955;
X.Y.Wu et al., Phys. Rev. Lett. **69** (1992) 1729;
S.D. Henderson et al., Phys. Rev. Lett. **69** (1992) 1733.

[6] E. Widmann et al., Z. phys. **A340** (1991) 209;
W.H. Trzaska et al. Phys. Lett. **B269** (1991) 54.

[7] A. Konaka et al., Phys. Rev. Lett. **57** (1986) 659;
M. Davier et al., Phys. Lett. **B180** (1986) 295;
C.N. Brown et al., Phys. Rev. Lett. **57** (1986) 2101;
E.M. Riordan et al., Phys. Rev. Lett. **59** (1987) 755;
A. Bross et al., Phys. Rev. Lett. **67** (1991) 2942.

[8] Y. N. Pokotilovskii, Phys. Part. Nucl. **24** (1993) 1.

[9] A. Schaeffer, Phys. Lett. **B211** (1988) 207;
E. Schramm et al. Mod. Phys. Lett. **A3** (1988) 783;
S. Graf et al., J. Phys. **G15** (1989) 1467;
E. Stein et al., Z. Phys. **A340** (1991) 377.

[10] W. Koenig and M. Tsertos, Phys. Rev. Lett. **68** (1992) 1959.

[11] W. Greiner, B. Mueller, J. Rafelski: Quantum Electrodynamics of Strong Field (1985) Springer-Verlag, Berlin.

[12] A. Belkacem et al., Phys. Rev. Lett. **58** (1987) 1196;
J.F. Bak et al. Phys. Lett. **B202** (1988) 615.

[13] G. Bassompierre et al., Europhysics Lett. **22** (1993) 239. In this paper there are misprints in the caption for Fig. 2: the number of Monte Carlo events for the continuous line is 2.8×10^3; for the dashed line 4.5×10^4.

[14] J. C. Kimball et al, Phys. Rev. Lett. **50** (1983) 950.

[15] J. Lindhard, Kong. Danks Vidensk. Selsk. Mat. Fys. Medd. **34**, no. 14 (1965).

[16] A.I. Akhieser and N.F. Shul'ga, Sov. Phys. Usp. **30** (1987) 197.

[17] N.P. Klepikov, Zh. Eksp. Teor. Fiz. **26** (1954) 19;
V.N. Baier, V.M. Katkov, V.S. Fadin, Radiation of relativistic electrons, p. 176 (1973) Atomizdat, Moscou (in Russian);
W.Y. Tsai and T. Erber, Phys. Rev. **D10** (1974) 492.

[18] This electron beam was made available by the CERN–SPS team.

[19] R. Alberganti et al. Nucl. Instrum. Methods Phys. Res., **A248** (1986) 337.

[20] X. Artru et al., Phys. Lett. **B313** (1993) 483.

[21] X. Artru, Nucl. Instrum. Methods Phys. Res. **B48** (1990) 278.

[22] W. R. Nelson et al., The EGS4 Code System. SLAC Report 265, 1985.